[18F]-FDG uptake in brain slices prepared from an aged mouse model of Alzheimer's disease using a dynamic autoradiography technique

Hiroko Maruyama (maruyama@ahs.kitasato-u.ac.jp)
Kitasato University
Misaki Gomi
Kitasato University
Thet-Thet Lwin
Kitasato University
Akio Yoneyama
Saga Light Source, Kyushu Synchrotron Light Research Center
Toru Sasaki
Kitasato University

Research Article

Keywords: Alzheimer's disease , [18F]-FDG-PET , Bioradiography, X-ray Phase-contrast imaging, Amyloid-β42, Tau protein

Posted Date: August 7th, 2023

DOI: https://doi.org/10.21203/rs.3.rs-3223282/v1

Version of Record: A version of this preprint was published at Annals of Nuclear Medicine on November 3rd, 2023. See the published version at https://doi.org/10.1007/s12149-023-01879-0.

Abstract

Objective

2-[^{18}F]fluoro-2-deoxy-D-glucose Positron Emission Tomography ([^{18}F]-FDG-PET) is a imaging modality that has been used to measure of glucose metabolism in the brain in Alzheimer's disease (AD). Clinically, decreased glucose uptake has been reported in the brain of AD, although the precise underlying mechanisms have not yet been elucidated. To elucidate the mechanisms of decreased [^{18}F]-FDG uptake in the AD by PET, [^{18}F]-FDG uptake in the brain of aged model mouse of AD was investigated using a dynamic autoradiography technique "bioradiogaraphy". A X-ray phase-contrast imaging (X-PCI) and a histopathological evaluation were also investigated to elucidate the mechanisms underlying the relationships between decreased [^{18}F]-FDG uptake and the pathological changes in the brain of AD mouse.

Methods

In this study, AD model mouse (APP^{+}/PS1^{+}) were used. [^{18}F]-FDG-bioradiography was conducted in fresh slices of brain tissue under the condition of resting (slices immersed in 5 mM K^{+} solution) and metabolically active (in 50 mM K^{+} solution). Amyloid β42 (Aβ42) deposition in the brain of AD mouse was confirmed by X-PCI. In addition, the positive cells of phosphated tau protein (P-tau) and deposition of Aβ42 were also examined by immunohistochemical staining.

Results

In the metabolically active condition, [^{18}F]-FDG uptake was significantly enhanced in the WT mouse but not significant in the AD mouse, whereas in resting condition, no significant difference was observed between two groups. In X-PCI showed Aβ deposition in the AD mouse, but not in the WT. The AD mouse also showed increased P-tau, accumulation of Aβ42, increase in neuronal apoptosis, and decrease in the number of neurons than that of the WT mouse.

Conclusion

Neuronal damage, and induction of neuronal apoptosis, decreased [^{18}F]-FDG uptake, increased Aβ accumulation and P-tau induced neurofibrillary degeneration are observed in AD mouse. In clinical diagnosis, reduction of [^{18}F]-FDG uptake by PET is one of the means of diagnosing the onset of AD. Our results suggest that decreased uptake of [^{18}F]-FDG in the brains of AD may be associated with neuronal dysfunction and cell death in the brain.

Introduction

Alzheimer's disease (AD) accounts for 60%-80% of all cases of dementia [1]. Since AD progresses with aging, it is feared that the number of AD patients will increase further in the future with the transition to a

super-aged society in Japan. As the number of patients is expected to continue to increase in the future, early diagnosis would be of importance [2, 3]. Recently, 2-[^{18}F]fluoro-2-deoxy-D-glucose-Positron Emission Tomography ([^{18}F]-FDG-PET) was reported as an excellent diagnostic tool for AD patient [4]. Glucose is taken up by the nerve cells of the brain through ATP generation and used as an energy source, as well as the generation of neurotransmitters [5]. The positron nuclide ([^{18}F]) used in PET emits minute amounts of radiation called gamma rays, which are detected by PET scanning and visualized on PET images. The image shows the amount of [^{18}F]-FDG uptake by the neurons in the brain. In other words, the activity of the whole brain can be visualized by the amount of [^{18}F]-FDG uptake. Healthy nerve cells require large amounts of sugar. Therefore, a healthy person's brain accumulates a large amount of the PET nuclide. It can be inferred that glucose metabolism is normal and the nerve cells undamaged and functioning normally in areas of the brain showing normal accumulation of [^{18}F]-FDG. The brains in AD patients, on the other hand, take up less glucose ([^{18}F]-FDG) than normal, due to the reduced neuronal metabolic activity associated with neuronal loss in this disease. Therefore, lower amounts of [^{18}F]-FDG are taken up by the brain in patients with AD, and PET images reveal areas of reduced [^{18}F]-FDG uptake: it is considered that the functions of the nerve cells are declining or that the nerve cells are missing in the parts showing reduced [^{18}F]-FDG uptake. Based on this principle, [^{18}F]-FDG-PET has become one of the most important tests for examining the severity of brain dysfunction in patients with AD [6]. [^{18}F]-FDG-PET is a useful diagnostic test for AD in humans, and has been reported to show evidence of hypometabolism in the cingulate cortex, parietotemporal lobe, and frontal lobe in patients with AD [6, 7]. Other diagnostic modalities, such as brain computed tomography (CT) and magnetic resonance imaging (MRI), have reported that hippocampal atrophy and Para hippocampal atrophy are more pronounced in AD brains than in normal brains [8]. On the other hand, it has been reported that [^{18}F]-FDG uptake is higher in the early stage of AD mice than in the WT mice [9]. A longitudinal PET imaging study of changes in cerebral glucose metabolism in AD mice reported decreased uptake of [^{18}F]-FDG in aged mice [10]. Behavioral analysis of AD mice and changes in the serum levels of inflammatory cytokines in relation to [^{18}F]-FDG imaging have also been reported [9, 11].

Therefore, we planned this study to clarify the differences in the uptake of [^{18}F]-FDG in the resting and metabolically active states in normal and AD brains, to accurately confirm the changes in the brain functions in AD. Towards this end, we performed [^{18}F]-FDG-PET imaging in the resting and metabolically active states of brain slices obtained from transgenic mouse models of AD and normal mice. We also analyzed brain damage by X-ray phase-contrast imaging (X-PCI) and immunohistochemical (IHC) staining to detect Aβ42 deposition and phosphorylated tau protein (p-tau). In addition, we also analyzed apoptotic neuronal cell death by in situ hybridization.

Material and methods

Animal experiment

The mice used in this study were generated by mating transgenic B6SJL-Tg6799 mice (The Jackson Laboratory, Bar Harbor, Me, USA) carrying the Alzheimer disease (AD) genes amyloid precursor protein (*APP*) and presenilin 1 (*PS1*), and female C57BL/6J female mice; female mice carrying the *APP* and *PS1* genes were used as the AD mice, and mice not carrying either the *APP* or a *PS1* gene were used as the wild type (WT) control mice. Experiments were conducted using female mice at 5 weeks of age, each experimental group consisting of 5 animals, each animal being housed in a small cage for 12 hours in a specific pathogen-free environment at 24°C, 50% humidity, and under a 12-hour light-dark cycle. The mice were weighed and fed once a week and dissected at 9 months of age. After deep isoflurane anesthesia (FUJIFILM Wako Pure Chem. Co., Osaka, Japan), blood was drawn from the mouse heart. The brains were cooled under ice for observation with 2-[^{18}F]fluoro-2-deoxy-D-glucose ([^{18}F]-FDG). Other brains were fixed in 4% paraformaldehyde in phosphate buffer (PFA, pH 7.3), and used as samples for X-PCI, and then embedded in paraffin. Blood samples were centrifuged at 3,500 rpm for 5 minutes at 4℃ and the separated serum samples were stored at − 80℃.

This study was conducted in compliance with the standards of the National Institutes of Health, and the Guidelines for handling radiopharmaceuticals Version 3.2 (Japanese Society of Nuclear Medicine), and an appropriate animal experiment plan has been approved by Animal Experimental Committee, Radiation Use Committee of the Faculty of Hygienic Sciences, Kitasato University (Medical Research Institute 16-03-5); approval was also obtained from, and approved by the High Energy Accelerator Research Organization (KEK).

Measurement of blood glucose and Glucagon-like peptide-1

The blood was collected from the mouse's tails vein to measure using a glutest neo-alpha glucometer (Sanwa Chemical Institute, Kanagawa, Japan). In addition, serum levels of the hormone, glucagon-like peptide-1 (GLP-1), which is secreted from the small intestine after a meal and functions to promote insulin secretion, were measured using an ELISA kit Wako (FUJIFILM Wako Pure Chem. Co.) (n = 5).

[^{18}F]-**FDG**-Bioradiography

The mice were deeply anesthetized with isoflurane (FUJIFILM Wako Pure Chem. Co.), whole blood was drained from the heart, and the brains were dissected out (n = 5). The mouse brains were then cross-sectioned 2.3 mm posterior to the bregma. Fresh slices of cerebral tissue (thickness: 300 μm) were then prepared with a micro slicer (Microslicer DTK-3000W; Dosaka EM, Kyoto, Japan) under ice cooling, immersed in the control Krebs-Ringer solution (5mM K^+-Krebs-Ringer solution: 124 mM NaCl, 5 mM KCl, 1 mM $MgCl_2 \cdot 6H_2O$, 2 mM $CaCl_2$, 26 mM $NaHCO_3$, 10 mM D-glucose). The brain slices were preincubated with control Krebs-Ringer solution at 37℃ under a continuous flow of 95% O_2/5% CO_2 gas was supplied to the solution. There were two incubation conditions, control and high K^+. The chamber for control condition was filled with 50 mL of control Krebs-Ringer solution, and that for high K^+ was with high K^+ Krebs-Ringer solution (79 mM NaCl, 50 mM KCl, 2 mM $CaCl_2$, 1 mM $MgCl_2$, 1.2 mM KH_2PO_4, 26 mM $NaHCO_3$ and 10 mM glucose), and placed them in the incubator at 37°C with a continuous flow of 95%

O_2/5% CO_2 gas was supplied to the solution. A set of eight brain slices WT or AD mouse was transferred on a nylon net in the chamber as shown in Fig. 3 and incubated with 18.5 MBq of [^{18}F]-FDG (FUJIFILM Toyama Chem. Co., Ltd., Tokyo, Japan) for 310 min. Two-dimensional images of radioactivity in the slices were recorded on radioluminography plate (CR plate; REGIUS RP-4S 8×10 cm; KONICA MINOLTA JAPAN, INC., Tokyo, Japan) without a cassette (REGIUS RP4S110; KONICA MINOLTA JAPAN, INC., Tokyo, Japan) through a thin polyvinylidene chloride sheet placed at the bottom of the chamber. Dynamic changes of radioactivity in the slices were measured by exposing the CR plate for 10 min and exchanging it every hour a total of 6 times. Autoradiographic images recorded on the plate were read using a REGIUS MODEL 170. An ROI was placed in the brain slices and analyzed using the Image J software. [^{18}F]-FDG uptake was expressed as “photostimulated luminescence (PSL/pixel/min)”. For quantitative analysis, the values were decay-corrected and converted into 80-kV X-ray equivalent using the correction formula provided by the manufacturer (KONICA MINOLTA JAPAN, INC.) as described in previously [12] and expressed as “nGy/pixel/min”. The uptake rate of [^{18}F]-FDG was obtained by plotting the [^{18}F]-FDG uptake against the incubation time and expressed as “ΔnGy/pixel/min”.

X-ray Phase-contrast imaging

Mouse brains fixed with 4% PFA were imaged using a two-crystal X-ray interferometry-based X-PCI system permanently installed in the Photon Factory of KEK, Tsukuba, Japan [13]. An X-ray CCD camera with a pixel size of 13×13 mm^2 and field of view of 16×13 mm^2 was used. The X-ray energy was set at17.8 keV. The exposure time was 5 s per projection and the total number of projections was 250 over 180°. Aβ accumulation in the brains was analyzed using the image-manipulating software (NIH Image version 1.41, https://imagej.nih.gov/nih-image). After the imaging, the brain tissues were subjected to IHC staining for Aβ42 by the method described above.

Analysis of phosphorylated tau protein, and total tau protein in the brain by Western blot

The cerebral cortex portion of the brain was homogenized with an ultrasonic homogenizer (Handy Sonic model UR-20P (TOMY SEIKO Co. Ltd., Tokyo, Japan)). The protein concentration was determined using the NuPAGE™ LDS Sample Buffer (4X) (Thermo Fisher Scientific) (Walham, MA, USA). 5 μg/well of each protein was applied to a 4%-20% polyacrylamide gel, separated by SDS-PAGE, and transferred to a PVDF membrane (BIO-RAD, Hercules, CA, USA). Blocking was performed at room temperature for 1 hour with PVDF Blocking Reagent for Can Get Signal® (Toyobo Co. Ltd., Osaka, Japan). The primary antibody Eb mAb to tau (phospho tau S404, P-Tau), abcam, Cambridge, UK) (1:4000) was reacted at room temperature for 1 hour. After washing with TBS (BIO-RAD) (Hercules, CA, USA) and TBS-T prepared using Tween-20, Peroxidase AffiniPure Donkey anti-Rabbit IgG (H + L) (Jackson Immuno Research, West Grove, PA, USA) (1:15000) was reacted in the dark at room temperature for 1 hour. Visualization by fluorescence and chemiluminescence was conducted using an imaging system (LI-COR) (Lincoln, NE, USA) and quantification was performed using the Pierce™ ECL Plus Western Blotting Substrate (Thermo Fisher Scientific). HRP was inactivated with a mixture of 0.3% H_2O_2 (FUJIFILM Wako Pure Chem. Co.) and TBS.

In addition, the primary antibody Eb mAb to Tau (TAU-5: T-Tau. abcam) was used, and BMAL1 Antibody (Novus Biologicals, Centennial, CO, USA) was used for BMAL1 detection. β-Actin(13E5) Rabbit mAb (HRP Conjugate. Cell signaling) was used for detection of β-Actin, a protein marker. The detection method is the same as above.

Immunohistochemical staining for phosphorylated tau and amyloid β42

Paraffin-embedded tissue sections (2 μm) were prepared from brain tissues fixed in 4% PFA (n = 5), autoclaved (120°C for 15 minutes) for antigen retrieval, and then treated with 0.3% H_2O_2 in phosphate-buffered saline (PBS) to inactivate endogenous peroxidase. Blocking was performed with normal sheep serum (DAKO, Santa Clara, CA, USA) for 30 minutes at room temperature. Primary antibody (phosphorylated tau: Rb mAb to Tau S404, abcam; used at a dilution of 1:500) or Amyloid β42 (Aβ42) Rabbit Polyclonal Antibody (SIG-39131 SIGNET; used at a dilution of 1:500) (Signet Research Inc., Englewood, NJ, USA) was incubated overnight at 4 ℃. After washing with PBS, Simple Stain Mouse MAX-PO(R) (Nichirei Biosciences, Tokyo, Japan) was added dropwise and allowed to react at room temperature for 30 minutes. Color development was performed using 3,3'-diaminobenzidine tetrahydrochloride (DAB) (FUJIFILM Wako Pure Chem. Co.). Five areas of the cerebral cortex (area 54.6×20.6 μm^2) were photographed with an optical microscope FSX100 (OLYMPUS, Tokyo, Japan), and the number of p-tau cells were counted and the areas of Aβ accumulation were analyzed using an image-manipulating software (NIH Image version 1.41).

In situ staining by the TUNEL method

The number of apoptotic cells was determined by the terminal deoxynucleotidyl transferase-mediated deoxyuridine triphosphate-biotin nick end labeling (TUNEL) method (In situ Apoptosis Detection Kit, Takara Bio) in paraffin-embedded sections of the brain (n = 5). The TUNEL assay labels the 3'OH ends of fragmented DNA with 2'-deoxyuridine-5'-triphosphate (dUTP) and identifies apoptotic cells and tissues. Apoptotic cells were detected by staining with DAB. Five areas of the cerebral cortex (total area 1,125 μm^2) were photographed with an optical microscope FSX100 (OLYMPUS, Tokyo, Japan), and the number of apoptotic cells was analyzed using an image-manipulating software (NIH Image version 1.41, https://imagej.nih.gov/nih-image).

Measurement of Caspase-3

For apoptosis-inducing signaling pathway analysis, activated Caspase-3 was quantified using the Caspase-3/CPP32 Colorimetric Assay Kit (Bio Vision Inc., CA. USA).

Statistical analysis

All data are expressed as means ± standard errors of the mean (SEM). Statistical analysis was conducted using the t-test and one-way ANOVA with Tukey's test using Graphpad prism 8.0 (San Diego, CA, USA). P values of < 0.05 were considered as denoting statistical significance.

Results

Body weight and food intake

There was no difference in the food intake or degree of weight gain during the experimental period between the two groups of mice.

GLP-1 and blood glucose levels

The blood glucose levels in the WT and AD mice during normal feeding were1.44 and 1.41 mg/ml, respectively, with no significant difference between the two groups (Fig. 1a). This finding confirmed that the glucose metabolic systems in the two groups of mice were the same. It was also confirmed that in this mouse strain, there was no significant difference in the amount of GLP-1 secreted from the intestinal L cells between the two groups of mice (36.7 pg/ml in the WT mice and 41.1 pg/ml in the AD mice) (Fig. 1b).

Brain uptake of [^{18}F]-FDG

Using [^{18}F]-FDG-bioradiography, we analyzed the [^{18}F]FDG uptakes in the barain slices prepared from WT and AD brains in resting (5 mM K^+ supplementation) and metabolically active condition (50 mM K^+ supplementation) of brain metabolism. Both groups of mice showed increased brain uptake of [^{18}F]-FDG over time (Fig. 2). In the resting state, there was no significant difference observed in [^{18}F]-FDG uptake rate (0.097ΔnGy/pixel/min) between the WT and AD brains. However active condition, while the WT mice showed higher [^{18}F]-FDG uptake rate (0.199ΔnGy/pixel/min) as compared with that in the resting state of WT mice groups ($p < 0.0003$), significant difference in uptake between the two states was observed in the WT mice. (Fig. 3, 4) On the other hand, in AD mice under active condition, [^{18}F]-FDG uptake rate increased by 0.157 ΔnGy/pixel/min compared to resting condition (0.107 ΔnGy/pixel/min), but was not significant (Fig. 4).

X-ray phase-contrast imaging

Figure 5a is a X-PCI and many bright punctate regions are visualized in the AD mice brain, but not observed in the brains of WT mice (Fig. 5b). On the other hand, the absolute density values in the bright punctate region-free regions were similar between the AD and WT brains. The phase-contrast X-PCI and histopathological images allowed us to clearly visualize structures such as the epithelium, thalamus, hypothalamus, and hippocampus in the AD brains, with high contrast resolution. In addition, many bright punctate areas were also visualized in the cerebral cortex and hippocampus in the AD brains. Comparison of the histopathological and X-PCI images revealed that the bright spots in the X-PCI images were consistent with areas of deposition of amyloid plaques (Aβ42) in the brain (Fig. 6a, b).

Analysis of phosphorylated tau protein by Western blotting

Significant increase in the amount of phosphorylated tau protein was observed in the cerebral cortex in the AD brains as compared with the WT brains (2.073 in the AD brains as compared with 1.053 in the WT

brains) (Fig. 7; $p < 0.011$).

Immunohistochemical staining for p-tau and Aβ42 in the brain

Significant increase in tau protein phosphorylation was observed in the AD brains as compared with the WT brains (Fig. 8a, b). The number of cells containing p-tau was 13.4 in the WT brains versus 21.7 in the AD mice (Fig. 8c; $p < 0.0188$). These results were consistent with the results of the Western blot analysis. No Aβ42 deposition was observed in the WT brains, whereas Aβ42 plaque deposition was clearly observed in the AD brains (Fig. 9); the amyloid plaques were scattered in the cerebral cortex and hippocampus.

In-situ staining of apoptotic cells

Apoptotic cells were detected by in situ hybridization. Higher numbers of TUNEL-positive cells were found in the AD brains as compared with the WT brains, reflecting apoptotic cell death in AD (Fig. 10a, b). The number of apoptotic cells was 18.6 in the AD brains versus 11.3 in the WT brains, being significantly increased in the AD brains (Fig. 10c; $p < 0.0001$).

Measurement of Caspase-3

Caspase-3, a downstream region of the caspase pathway that induces apoptosis, was not different between WT mice and AD mice (Fig. 11).

Discussion

It has been reported that on [^{18}F]-FDG-PET, the amount of glucose ([^{18}F]-FDG) uptake in the brain is decreased in AD patients [14]. However, the relationship between the decreased [^{18}F]-FDG uptake on [^{18}F]-FDG-PET and the histopathological changes remains unclear. Therefore, we investigated the correlation between the [^{18}F]-FDG uptake and the brain histopathological changes in the WT and AD mice brains. At the final stage of the experiment, we compared and confirmed the functional changes in the WT and AD mice brains associated with metabolic activity.

To begin the experiment, we measured the amount of gastrointestinal hormone (GLP-1) exerts its hypoglycemic effect through glucose-stimulated insulin secretion enhancement and glucagon suppression, secretes from intestinal L cells [15]. Our measurement revealed no difference in the serum levels of GLP-1 between the AD mice and WT mice. In addition, we also found no differences in the blood glucose levels between the WT mice and AD mice. Based on this result, we performed a comparative experiment of [^{18}F]-FDG uptake to investigate glucose metabolism in the WT and AD mice brains.

Cellular potassium channels are involved in the formation of the resting membrane potential, electrical cellular responses, synaptic transmission, and maintenance of potassium homeostasis [16]. Nerve cells are depolarized under high- potassium conditions, the cells becoming more reactive and entering a

hypermetabolic state [17]. Using this principle, we placed the brain in Krebs-Ringer solution containing 5 mM K+ (rest condition) or and 50 mM K+ (depolarized condition), and examined the differences in the brain glucose ([^{18}F]-FDG) uptake between the two conditions [12]. While [^{18}F]-FDG-PET is already in use clinically for the diagnosis of AD patient, the mechanism underlying the reduced glucose uptake in the AD brain remains unclear [18]. We attempted to elucidate the mechanism by which [^{18}F]-FDG-PET uptake is reduced in AD brains, making it an effective diagnostic tool for AD patient, through comparative experiments using AD mouse models. We also employed phase-contrast X-ray imaging, immunohistochemical staining and biochemical methods to clarify whether any associations existed between the immunohistopathological changes in the brain and the reduced [^{18}F]-FDG uptake in AD mouse. The characteristic pathological findings in AD patients are the formation of neurofibrillary tangles (tau pathology) and the deposition of senile plaques (amyloid-β peptide) in the brain, hypothesized as being the result of the so-called tau and amyloid cascades [19, 20]. Phosphorylation of tau protein, one of the microtubule-associated proteins involved in extraneuronal deposition, also leads to the formation of neurofibrillary tangles that aggregate and lead to neuronal cell death [20]. Elucidation of the transition mechanism from tau pathology to amyloid pathology and the complex mechanisms underlying neuronal cell death in AD is also ongoing [21]. While it has become clear that tau protein phosphorylation and amyloid deposition influence the onset and exacerbation of AD, the relationships between brain [^{18}F]-FDG uptake and these pathological changes remains unclear. Treatment of WT brain slices with 50 mM K^+ Krebs-Ringer solution led to a significantly increased [^{18}F]-FDG uptake as compared with the addition of 5 mM K^+ Krebs-Ringer solution. On the other hand, following exposure to 50 mM K^+ Krebs-Ringer solution, the uptake rate of [^{18}F]-FDG in the AD brains was suppressed as compared with that in the WT brains. This result suggested abnormal synaptic transmission in the AD brains associated with glucose metabolic dysfunction. Excessive phosphorylation of tau protein is known to cause structural abnormalities and neurofibrillary degeneration [22]. To investigate the cause of the decreased [^{18}F]-FDG uptake in the AD brains, we examined the brains for neurofibrillary tangles and the presence of senile plaques (Aβ), the hallmark lesions associated with functional decline in AD. In Western Blotting and HIC stain, an p-tau-positive cells are increased in AD brains as compared with the WT brains. Increased accumulation of phosphorylated tau has been reported to destabilize axons and cause neurofibrillary degeneration [23, 24]. In this experimental system, Aβ aggregation could be detected by phase-contrast X-ray CT imaging, which revealed amyloid plaques as bright spots. The locations of the bright spots were almost the same as those of the amyloid plaques observed by IHC staining. This suggests the possibility of using phase-contrast X-ray CT 19imaging for drug discovery and diagnosis in the future. Amyloid deposition in the early stages of AD development is deeply involved in the induction of Tau protein phosphorylation [25]. That confirmation of Aβ deposition is important in terms of suppressing progression of AD pathology.

Based on these reports, when the neuronal apoptotic activity was measured by TUNEL assay, a significant increase in the number of apoptotic cells was observed in the AD brains as compared with the WT brains. It has been reported that the action of caspases are a family of proteases that play a central

role in many vital processes, including cell death and inflammation. Caspase-3, a key regulator of the apoptotic response, has been identified as one of the key mediators of apoptosis [26, 27, 28]. In addition, since apoptosis was induced in neurons, but no difference of caspase-3 was observed between the WT brains and AD brains. However, since there are other apoptosis-inducing pathways, there is a possibility that it was induced by a different pathway.

Tau protein phosphorylation and Aβ aggregation in the brain have been reported to activate inflammatory responses and damage synaptic transmission systems [29]. Although the activated microglia by inflammatory cannot directly induce neuronal apoptosis, but there are reported the number of activated microglia is correlating with the neuron loss increases with age [30, 31].

It has been reported that the presence of tau protein is important in clinical studies, where FDG uptake is decreased in glucose metabolism in the brains of AD patients [32, 33]. Increased phosphorylation of tau protein and microtubule-associated protein, has been reported to destabilize axons and cause neurofibrillary degeneration [23]. Degeneration of cerebral nerve cells and induction of cell death must inevitably lead to a decrease in the activity of glucose metabolism in the brain.

Based on the results of the present study, AD-induced decline in brain function appears to be greatly influenced by the induction of apoptosis by excess phosphorylated tau protein and Aβ accumulation. We concluded from these results that decreased uptake of [^{18}F]-FDG in the AD brain may be caused by a decrease in neuronal function and number of neuron loss in the brains of the AD mice. Early identification of the relationship between activated microglia/tau protein phosphorylation and neuronal cell death is needed.

Conclusion

In conclusion, comparative analysis of [^{18}F]-FDG uptake between the brains of WT and aged AD mice revealed no significant difference in resting-state uptake between the two groups. The results revealed that, it was revealed that glucose metabolism in the brain was significantly decreased in AD mice compared to WT mice under metabolic activation conditions. Therefore, to diagnose AD based on differences in [^{18}F]-FDG uptake in the brain, it is important to assess [^{18}F]-FDG uptake in a metabolically active state.

Aβ accumulation occurred in aged AD mice, leading to increased phosphorylated tau protein and neurodegeneration in AD mouse brains, with apoptotic neuronal cell loss. These results suggest that Aβ is involved in the induction of phosphorylation of tau protein in the later stages of AD, directly affecting neuronal damage, and reducing the intake of glucose, the energy source of the brain. However, a direct reduction in [^{18}F]-FDG uptake at sites of amyloid accumulation in the brain could not be confirmed.

Declarations

Acknowledgements

This work was supported by JSPS KAKENHI Grant Number JP18K11108.

Data availability statement

All data used to support the findings of this study are included within the article.

Conflict of interest

There are no conflicts of interests to declare. The authors declare that they have no known competing financial interests or personal relationships that could have potentially influenced the work reported in this paper.

Funding statement: The author(s) received no financial support for the research, authorship and/or publication of this article.

References

1. 2022 Alzheimer's disease facts and figures. Alzheimer's Dementia® The Journal of The Alzheimer's Association. 2022;703.
2. Gauthier S, Rosa-Neto P, Morais JA, Webster C. World Alzheimer Report 2021: Journey through the diagnosis of dementia. London, England: Alzheimer's Disease International.
3. McDade E, Bateman RJ. Stop Alzheimer's before it starts. Nature. 2017;547:153–5.
4. Mosconi L, Tsui HW, Hesholz K, et al. Multicenter standardized ^{18}F-FDG PET diagnosis of mild cognitive impairment, Alzheimer's disease, and other dementias. J Nucleare Medi. 2008;49(3):390–8.
5. Mergenthaler P, Lindauer U, Dienel GA, Meisel MA. Sugar for the brain: the role of glucose in physiological and pathological grain function. Trends Neurosci. 2013;36(10):587–97.
6. Mosconi L. Brain glucose metabolism in the early and specific diagnosis of Alzheimer's disease FDG-PET studies in MCI and AD. Eur J Nucl Med Mol Imag. 2005;32:486–510.
7. Bohnen NI, Djang DSW, Herholz K, Anzai Y, Minoshima S. Effectiveness and safety of 18F-FDG PET in the evaluation of dementia: A review of the recent literature. J Nucl Med. 2012;53(1):59–71.
8. Vemuri P, Wiste HJ, Weigand SD, Shaw LM, Trojanowski JQ, Weiner MW, et al. MRI and CSF biomarkers in normal, MCI, and AD subjects: predicting future clinical change. Neurol. 2009;73(4):294–301.
9. Li XY, Men WW, Zhu H, Lei JF, Zuo FX, Wang ZJ, et al. Age- and brain region-specific changes of glucose metabolic disorder, learning, and memory dysfunction in early Alzheimer's disease assessed in APP/PS1 transgenic mice using ^{18}F-FDG-PET. Int J Mol Sci. 2016;17(10):1707.
10. Takkinen JS, López-Picón FR, Al Majidi R, Eskola O, Krzyczmonik A, et al. Brain energy metabolism and neuroinflammation in ageing APP/PS1-21 mice using longitudinal ^{18}F-FDG and ^{18}F-DPA-714

PET imaging. J Cereb Blood Flow Metab. 2017;37:2870–82.

11. Patel NS, Paris D, Mathura V, Quqdros AN, Crawford FC, Mullan MJ. Inflammatory cytokine levels correlate with amyloid load in transgenic mouse models of Alzheimer's disease. J Neuroinflamme. 2005;2:9.
12. Sasaki T, Tamaki J, Nishizawa K, Kojima T, Tanaka R, Moriya R, et al. Evaliation of cell viability and metabolic activity of 3D cultured human epidermal model using a dynamic autoradiographic techinique with a pet radiopharmaceutical. Scien Rep. 2019;9:10685.
13. Yoneyama A, Takeda T, Tsuchiya Y, Wu J, Lwin TT, Hyodo K, et al. High-energy phase-contrast X-ray imaging using a two-crystal X-ray interferometer. J Synchrotron Rad. 2005;12:534–6.
14. Minoshima S, Cross D, Thientunyakit T, Foster NL, Drzezga A. ^{18}F-FDG PET imaging in neurodegeneration dementing disorders: insights into subtype classification, emerging disease categories, and mixed dementia with copathologies. J Nucl Med. 2022;63:2S–12S.
15. Tolhurst G, Reimann F, Gribble FM. Nutritional regulation of glucagon-like peptide-1 secretion. J Physiol. 2009;581(1):27–32.
16. Andrew RD, Hsieh Y-T, Brisson CD. Spreading depolarization triggered by elevated potassium is weak or absent in the rodent lower brain. J Cereb Blood Flow Metab. 2017;37(5):1735–47.
17. Higashi K, Fujita A, Inanobe A, Tanemoto M, Doi K, Kubo T, et al. An inwardly rectifying K + channel, Kir4.1, expressed in astrocytes surrounds synapses and blood vessels in brain. Am J Physiol Cell Physiol. 2001;281:C922–C31.
18. Rosa PAD, Cerami C, Gallivanone F, Prestia A, Caroli A, Castiglioni I, et al. A standardized [^{18}F]-FDG-PET template tor spatial normalization in statistical parametric mapping of dementia. Neuroinform. 2014;12:575–93.
19. Karran E, Mercken M, Strooper BD. The amyloid cascade hypothesis for Alzheimer's disease: an appraisal for the development of therapeutics. Nat Reviws. 2011;10:698–712.
20. Arnsten AFT, Datta D, Tredici KD, Braak H, Hypothesis. Tau pathology is an initiating factor in sporadic Alzheimer's disease. Alzheimer's Dementia® J Alzheimer's Associa. 2020;17(1):1–139.
21. Hashimoto S, Matsuba Y, Kamano N, Mihira N, Sahara N, Takano J, et al. Tau binding protein CAPON induces tau aggregation and neurodegeneration. Nat Communi. 2019;10:2394.
22. Mandelkow EM, Mandelkow E. Biochemistry and Cell Biology of Tau Protein in Neurofibrillary Degeneration. Cold Spring Harb Perspect Med. 2012;2:a006247.
23. Iqbal K, Liu F, Grong CX, Grundke-Iqbal I. Tau in Alzheimer disease and related tauopathies. Curr Alzheimer Res. 2010;7(8):656–64.
24. Rawat P, Sehar U, Bisht J, Selman A, Culberson J, Reddy PH. Phosphorylated Tau in Alzheimer's Disease and Other Tauopathies. Int J Mol Sci. 2022;23:12841.
25. Wright AL, Zinn R, Hohensinn B, Konen LM, Beynon SB, Tan RP, et al. Neuroinflammation and Neuronal Loss Precede Ab Plaque Deposition in the hAPP-J20 Mouse Model of Alzheimer's Disease. PLoS ONE. 2013;8(4):e59586.

26. Poon CH, Wong STN, Roy J, Wan Y, Chan HWH, Steinbusch H, et al. Sex Differences between Neuronal Loss and the Early Onset of Amyloid Deposits and Behavioral Consequences in 5xFAD Transgenic Mouse as a Model for Alzheimer's Disease. Cells. 2023;12:780.
27. Sun X, Nie B, Zhao S, Ai L, Chen Q, Zhang T, et al. Distinct relationship of amyloid-beta and tau deposition to cerebral glucose metabolic networks in Alzheimer's disease. Neurosci Lett. 2020;717:13499.
28. Raina AK, Hochman A, Zhu X, Rottkamp CA, Nunomura A, Siedlak SL, et al. Abortive apoptosis in Alzheimer's disease. Acta Neuropathol. 2001;101(4):305–10.
29. Yang DS, Kumar K, Stavrides P, Peterson J, Peterhoff CM, Pawlik M, et al. Neuronal Apoptosis and Autophagy Cross Talk in Aging PS/APP Mice, a Model of Alzheimer's Disease. Am J Pathol. 2008;173(3):665–81.
30. Louneva N, Cohen JW, Han LY, Talbot K, Wilson RS, David A, et al. Caspase-3 is Enriched in Postsynaptic Densities and Increased in Alzheimer's Disease. Am J Pathol. 2008;173(5):1488–95.
31. Jembrek MJ, Hof PR, Šimić G. Ceramides in Alzheimer's Disease: Key Mediators of Neuronal Apoptosis Induced by Oxidative Stress and Aβ Accumulation. Oxid Med Cell Longev. 2015;2015:Article ID 346783, 17 pages.
32. Strom A, Iaccarino L, Edwards L, Lesman-Segev OH, Soleimani-Meigooni DN, Pham J, et al. Cortical hypometabolism reflects local atrophy and tau pathology in symptomatic Alzheimer's disease. Brain. 2022;145:713–28.
33. Bischof GN, Jessen F, Fliessbach K, Dronse J, Hammes J, Neumaier B, et al. Impact to tau and amyloid burden on glucose metabolism in Alzheimer's disease. Ann Clin Transl Neurol. 2016;3(12):934–9.

Figures

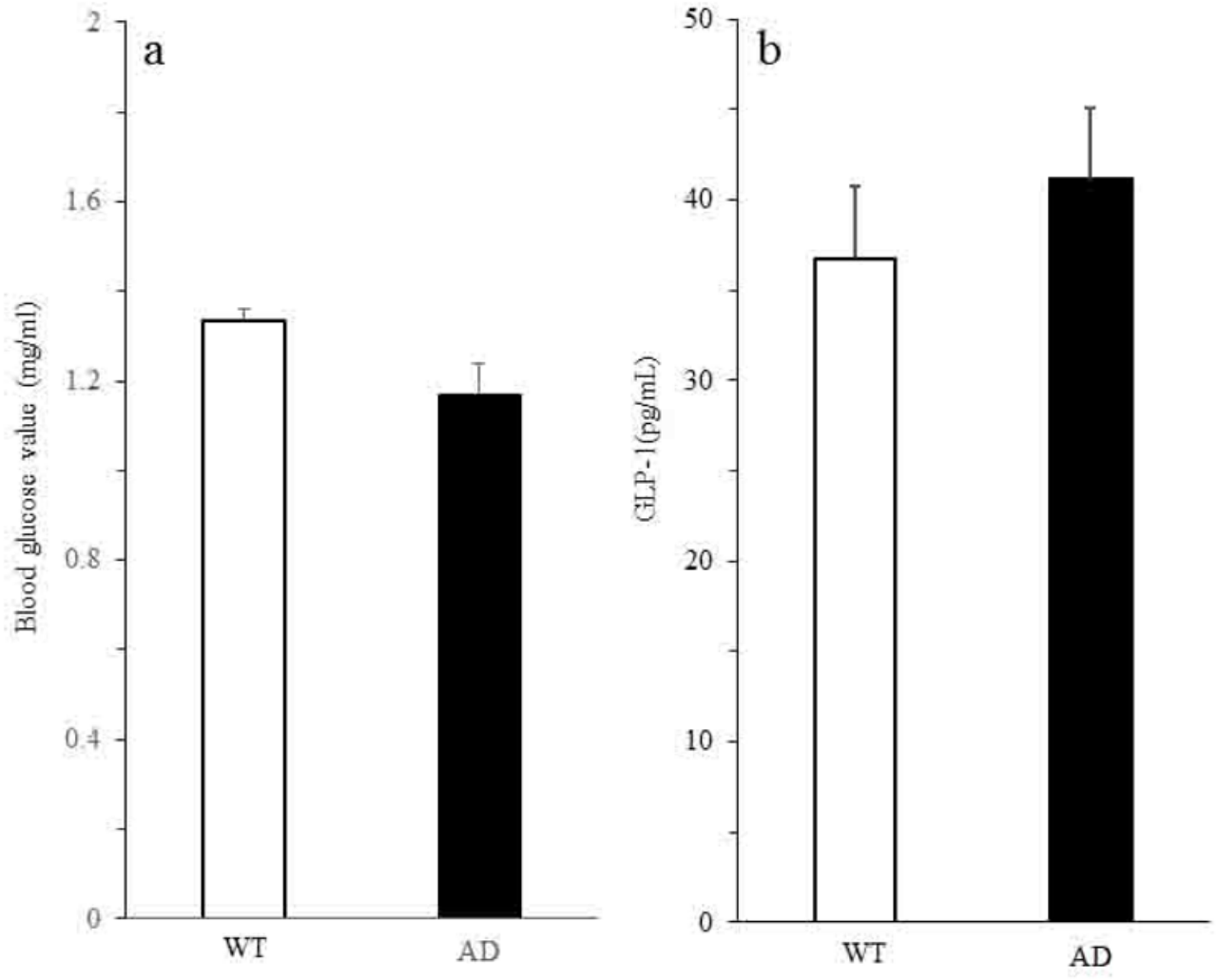

Figure 1

Measurement of the blood glucose levels and blood intestinal hormone (GLP1) levels in the experimental mice. (a) The blood glucose levels were measured at the end of the experiment using a glucometer in blood samples obtained from the mouse tails. (b) Serum GLP-1 was measured at the end of the experiment using an ELISA kit. The data are presented as means ± SE (n = 5).

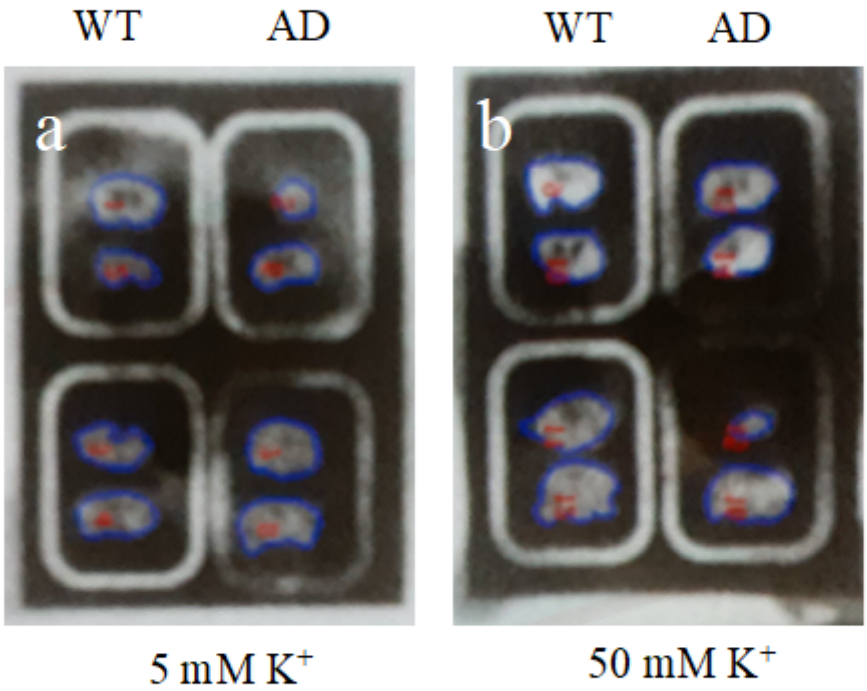

Figure 2

The [^{18}F]-FGD uptake levels were measured in brain slices immersed in Krebs-Ringer solution containing 5 mM K+ (a) or 50 mM K+ (b). The measurements were performed in regions of interest (ROIs) set in the acquired images using a radioluminography device, converted to the amount of stimulated luminescence per unit area, and corrected for radioactivity decay.

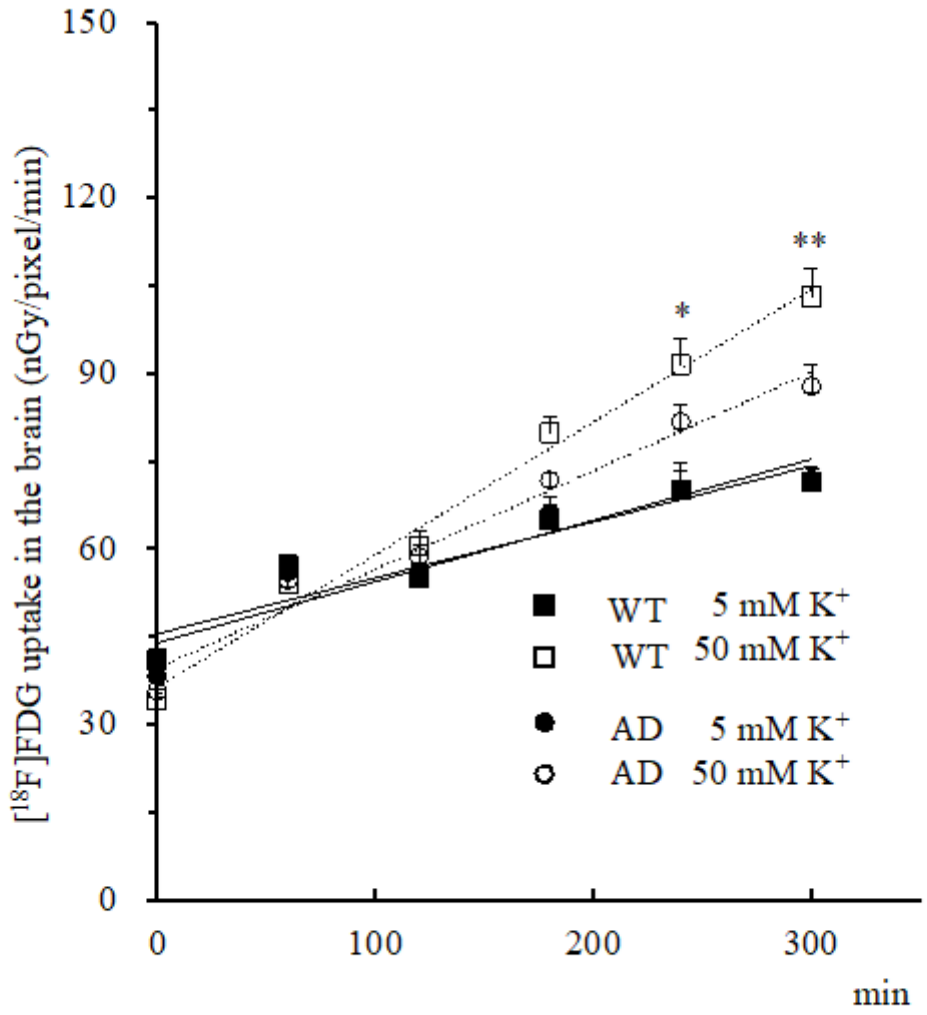

Figure 3

The uptake rate of [^{18}F]-FDG was defined as the rate of increase in photostimulated luminescence (PSL) per unit time (ΔPSL/mm^2/min), and the brain [^{18}F]-FDG uptake was expressed as “PSL/pixel/min”. Dynamic changes in the radioactivity in the tissues were measured by exposing the plates for 45 min and exchanging them every 60 min over a period of 405 min. For quantitative analysis, the values were expressed as “nGy/pixel/min”. The [^{18}F]-FDG rate was calculated by plotting the [^{18}F]-FDG uptake level against the incubation time and expressed as “ΔnGy/pixel/min”. Data are presented as means±SE (n = 5). * 240 min; WT 5 mM K+ vs. WT 50 mM K+: p = 0.0011, ** 300 min; WT 5 mM K+ vs. WT 50 mM K+: p = 0.0101.

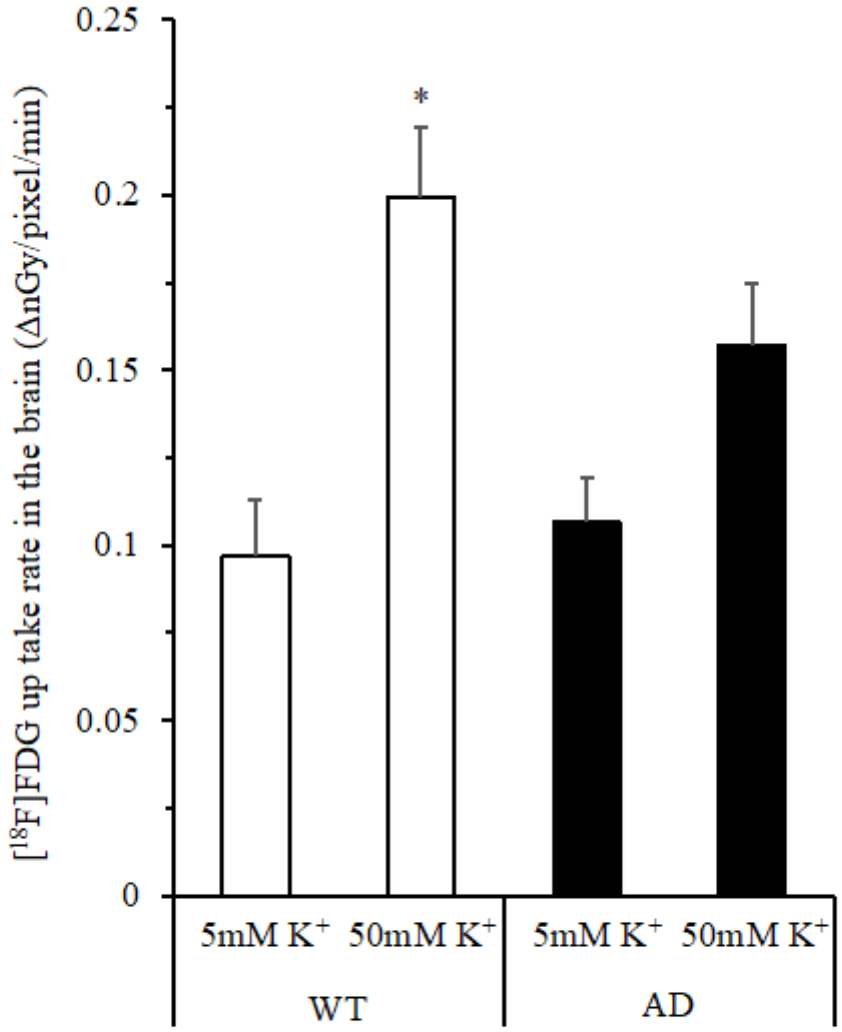

Figure 4

Measurement of [^{18}F]-FDG uptake in the whole mouse brain using [^{18}F]-FDG-Bioradiography. WT brains (white bars): The uptake was significantly increased in the brain slices immersed in 50 mM K^+ Krebs-Ringer solution as compared with those immersed in 5 mM K^+ Krebs-Ringer solution. AD brains (black bars): No significant difference in uptake was observed between brain slices immersed in 5 mM K^+ and 50 mM K^+ Krebs-Ringer solutions. Data are presented as means ± SE (n = 5). * p <0.0003 vs. WT 5 mM K^+.

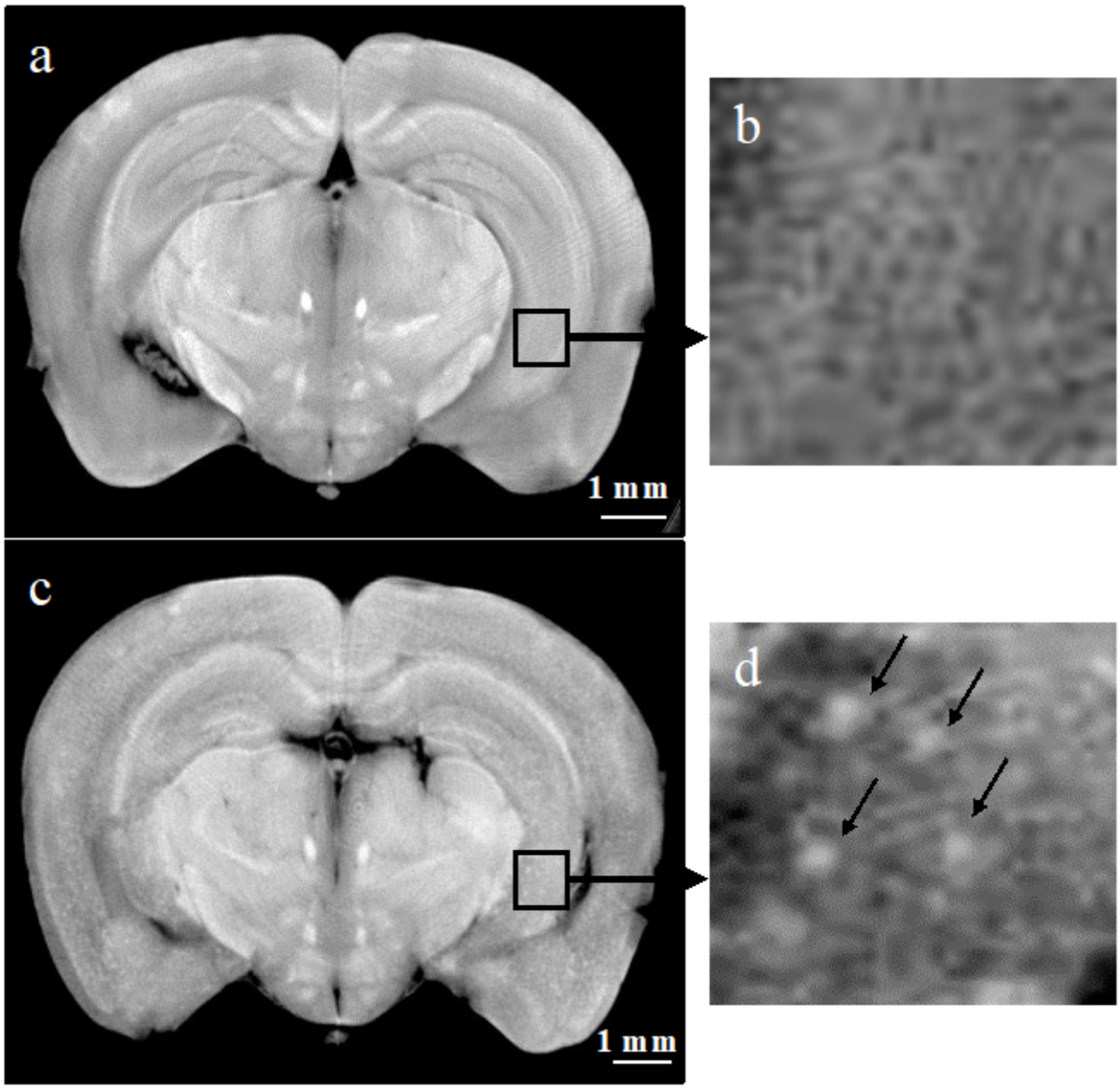

Figure 5

X-PCI using an X-ray interferometer was carried out in mouse brains fixed in 4% PFA. The imaging conditions were as follows: X-ray energy, 17.8 keV; number of projections, 250 projections/180°; pixel size, 13×13 μm^2; and imaging time, 30 seconds/projection. Aβ accumulation was analyzed using an image manipulation software (NIH Image version 1.41). (a) and (b): Images of the WT brains; (c) and (d): Images of the AD brains. Bright dots (arrows) were observed in the brains of AD mice.

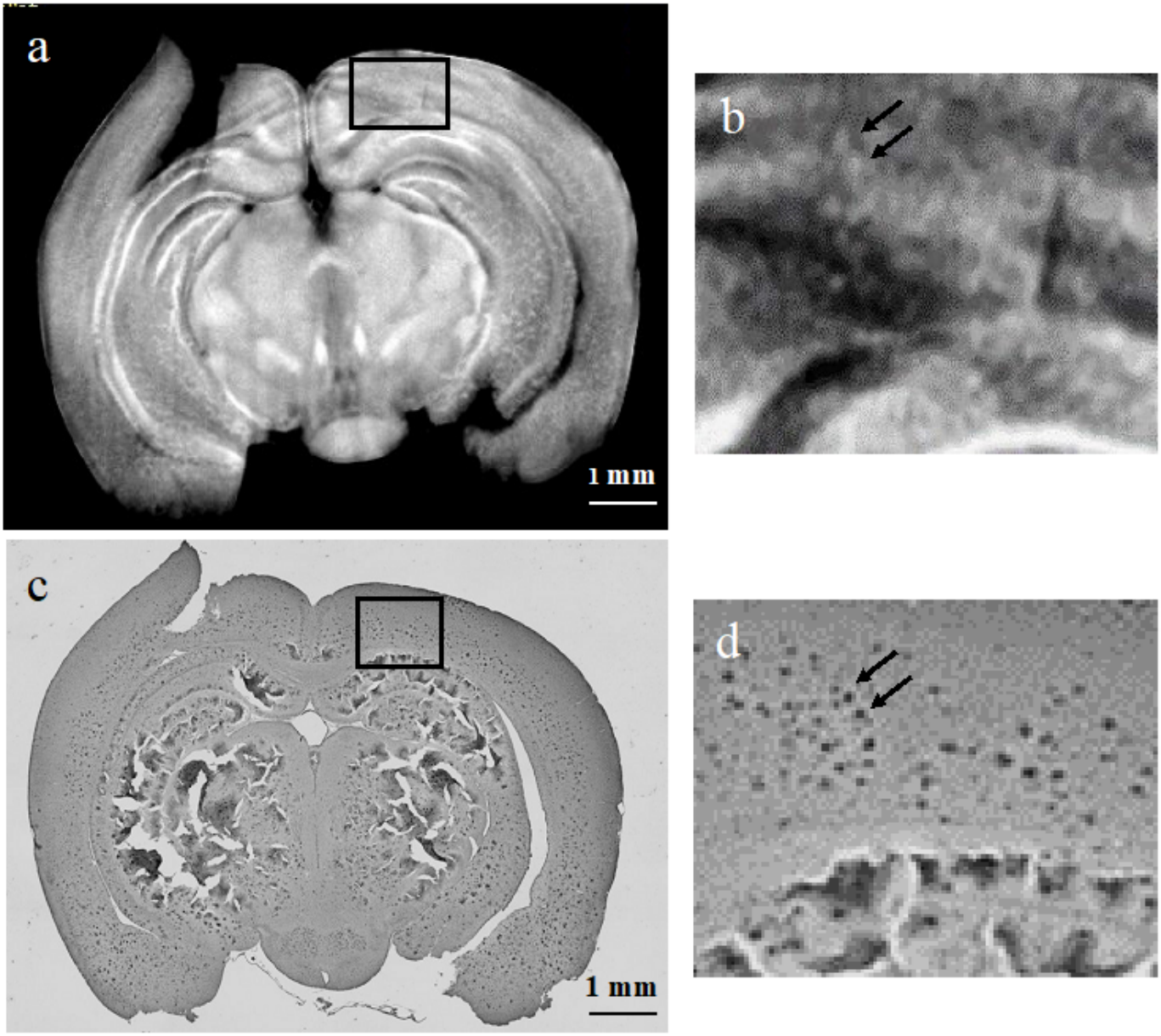

Figure 6

X-PCI of the same part of the AD brains. (a) and (b): X-PCI. Deposits of Aβ42 (arrow) are visualized as bright dots. (c) and (d): Aβ42 IHC images. Deposits of Aβ42 are visualized as black dots (arrow).

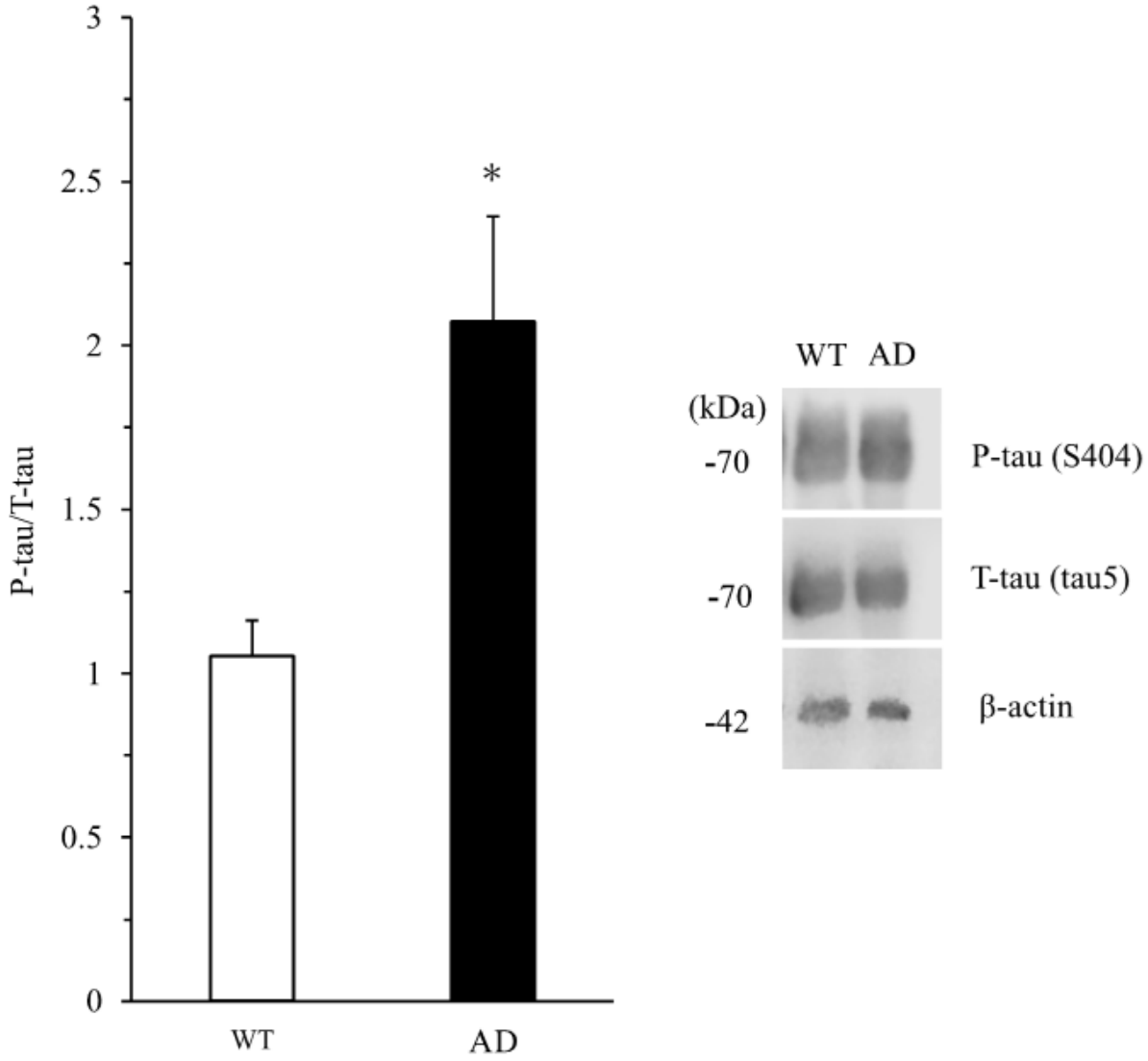

Figure 7

Phosphorylated tau protein accumulation was analyzed by Western blotting and expressed as the ratio of phosphorylated tau protein (p-tau) to total tau protein (T-tau), obtained by homogenizing the cerebral cortex. The intensities of the p-tau and t-tau bands were normalized to those of their respective total protein bands. Data are presented as means ± SE (n = 5). *p <0.011 vs. WT.

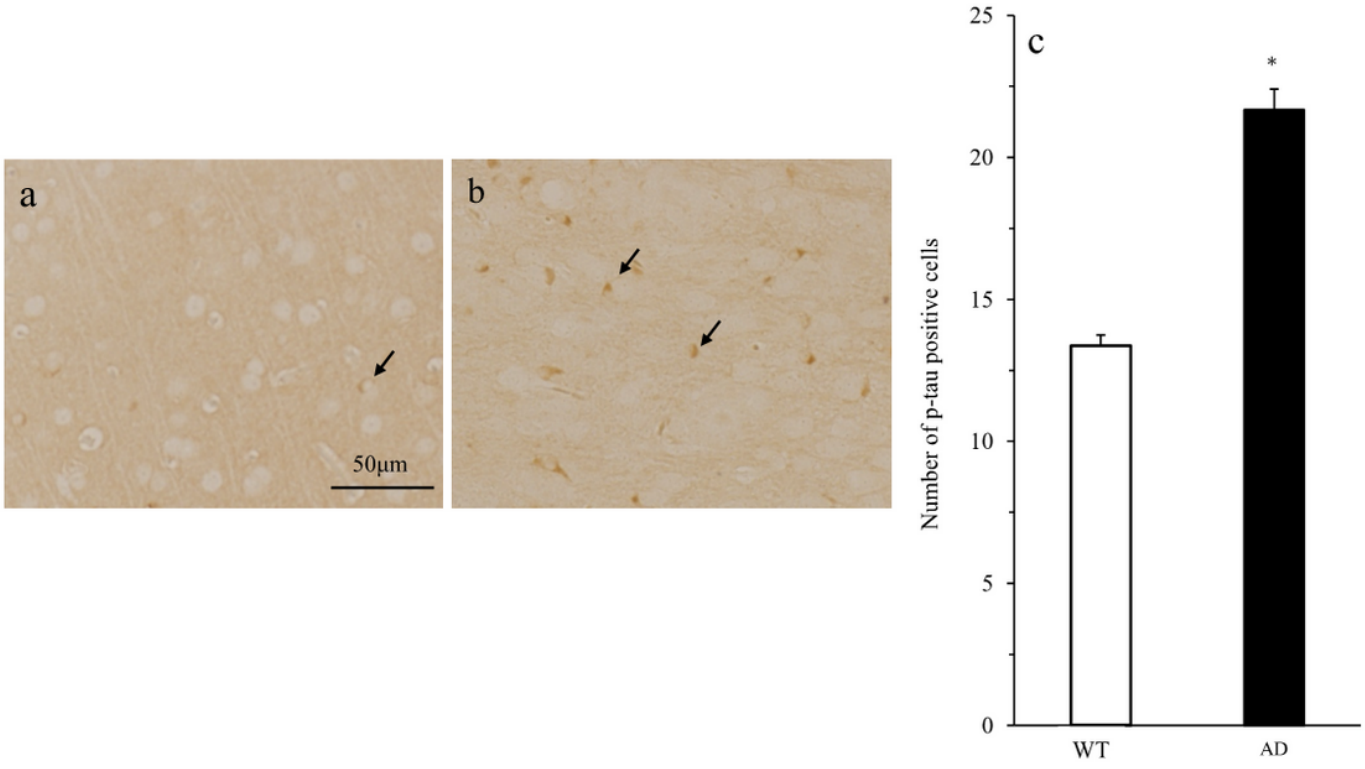

Figure 8

IHC staining of phosphorylated tau protein (S404). (a): WT brain; (b) AD brain. Arrows indicate phosphorylated tau protein-positive cells in the cerebral cortex. (c): The result of calculating positive cells within an area of 54.6×20.6 μm^2. Data are presented as means ± SE (n = 5). *p <0.0188 vs. WT.

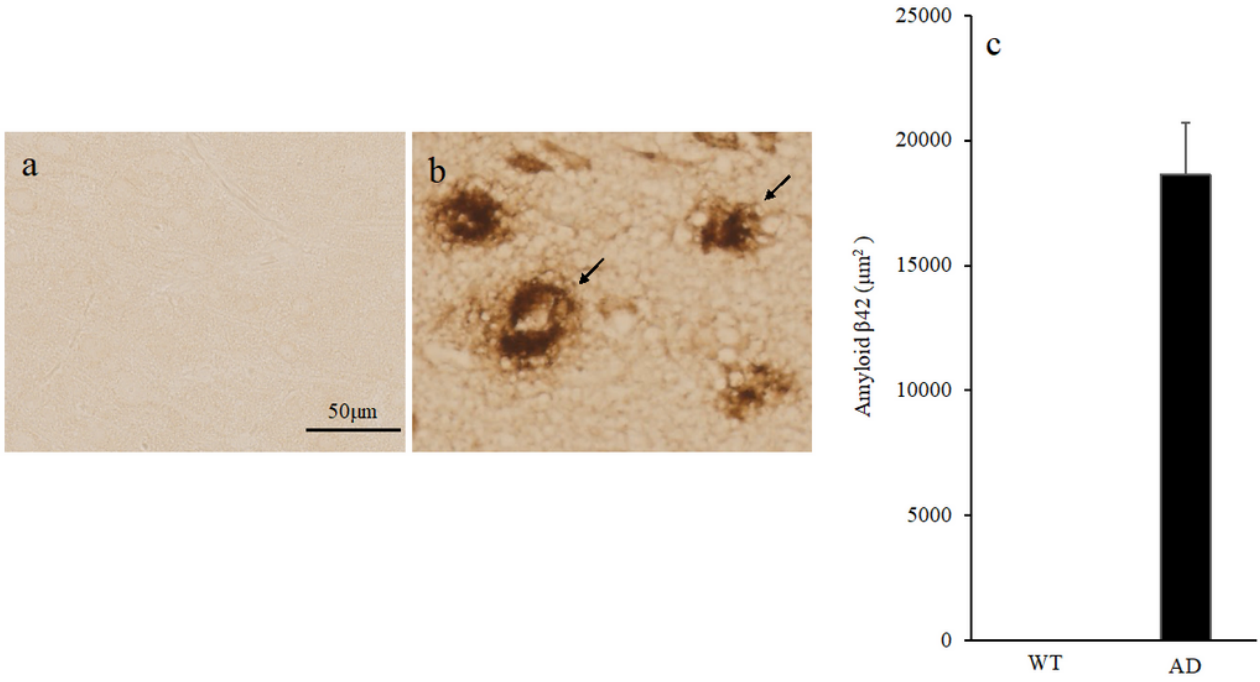

Figure 9

IHC staining of the cerebral cortex with Aβ42 antibody. (a) WT brain: Aβ42-positive areas are absent. (b) AD brains: Aβ42-positive (arrows) are clearly visible. (c): The figure represents the Aβ42 area calculated within a total area of 54.6 × 20.6 μm^2. Data are presented as means ± SE (n = 5).

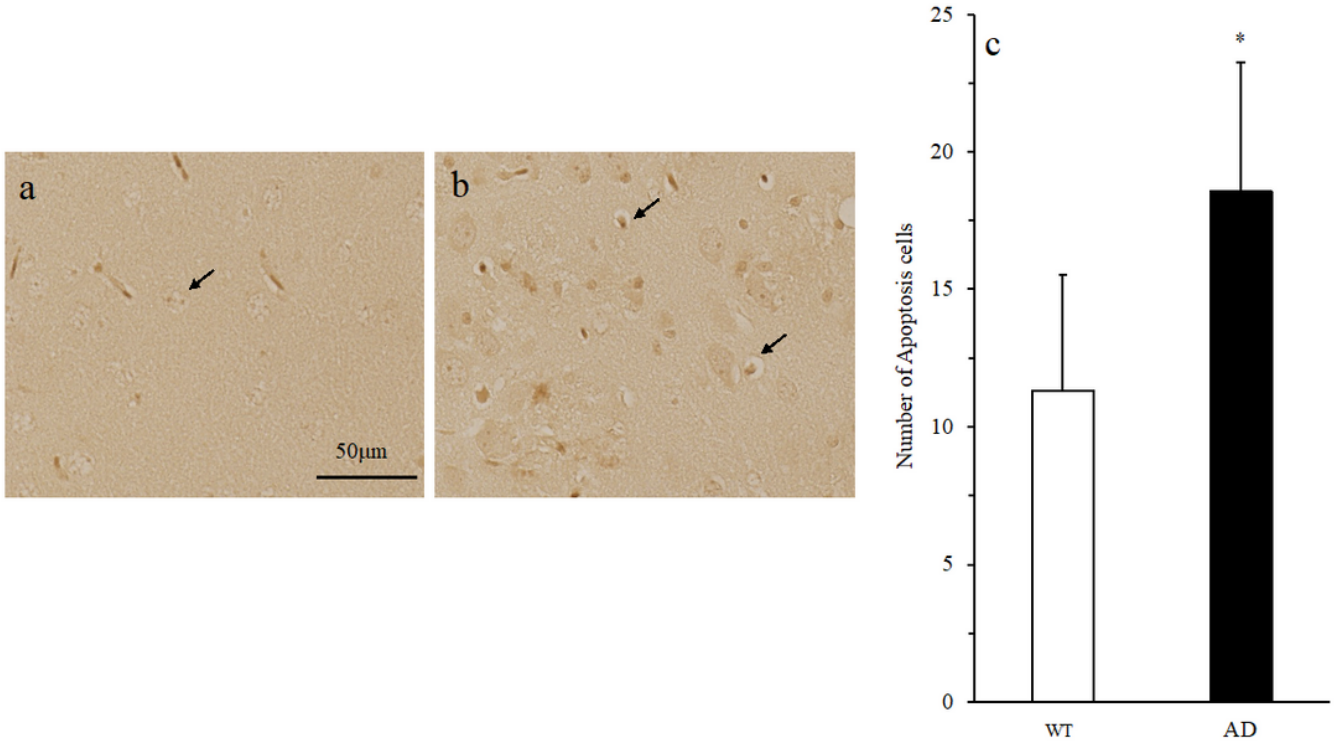

Figure 10

In situ detection (TUNEL method) of apoptotic cells (arrows). (a) WT brain. (b) AD brain. (c) The number of positive cells calculated in an area of 54.6×20.6 μm^2 in the brain. Data are presented as means ± SE (n = 5). *p <0.0001 vs. WT.

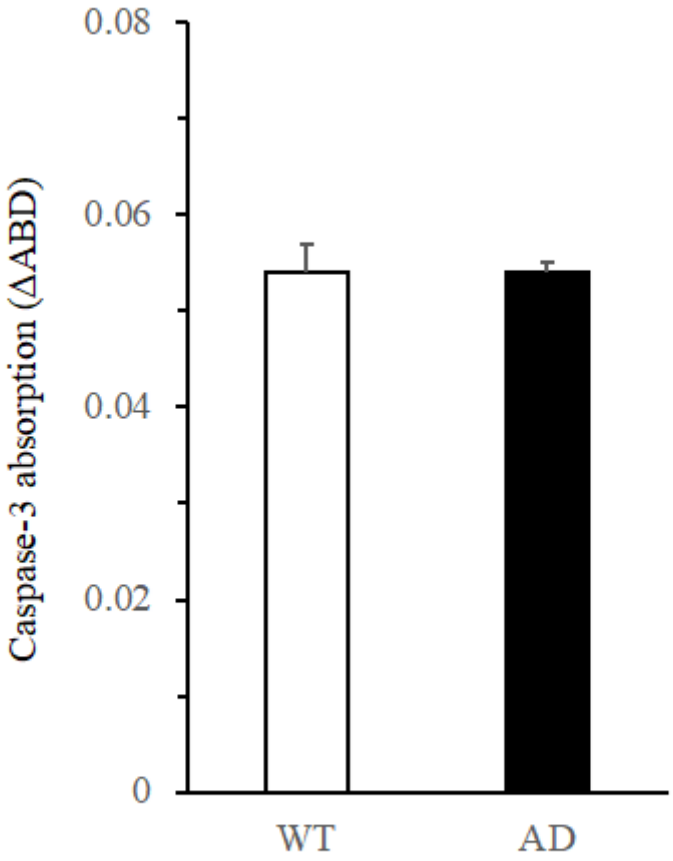

Figure 11

Caspase-3, which is one of the apoptosis-inducing factors in the brain, was measured using the Caspase-3/CPP32 Colorimetric Assay Kit. The figure is expressed as absorbance.